AGU PUBLICATIONS

JGR

Journal of Geophysical Research: Earth Surface

RESEARCH ARTICLE
10.1002/2015JF003593

Seasonal and diurnal cycles of liquid water in snow—Measurements and modeling

A. Heilig[1,2], C. Mitterer[3], L. Schmid[3], N. Wever[3,4], J. Schweizer[3], H.-P. Marshall[2], and O. Eisen[5,6]

[1]IUP Institute of Environmental Physics, Heidelberg, Germany, [2]Department of Geosciences, Boise State University, Boise, Idaho, USA, [3]WSL Institute for Snow and Avalanche Research SLF, Davos Dorf, Switzerland, [4]École Polytechnique Fédérale de Lausanne, School of Architecture, Civil and Environmental Engineering, Lausanne, Switzerland, [5]Alfred-Wegener-Institut Helmholtz Zentrum für Polar-und Meeresforschung, Bremerhaven, Germany, [6]Fachbereich Geowissenschaften, Universität Bremen, Bremen, Germany

Key Points:
- Liquid water in snow rarely exceeds 5 vol % in natural snowpacks
- Slopes and flat sites require different assumptions for holding capacities
- Outflow predictions are improved if knowledge on water retention is applied

Correspondence to:
A. Heilig,
heilig@r-hm.de

Citation:
Heilig, A., C. Mitterer, L. Schmid, N. Wever, J. Schweizer, H.-P. Marshall, and O. Eisen (2015), Seasonal and diurnal cycles of liquid water in snow—Measurements and modeling, *J. Geophys. Res. Earth Surf.*, *120*, 2139–2154, doi:10.1002/2015JF003593.

Received 23 APR 2015
Accepted 22 SEP 2015
Accepted article online 24 SEP 2015
Published online 20 OCT 2015

Abstract Evaluating and improving snow models and outflow predictions for hydrological applications is hindered by the lack of continuous data on bulk volumetric liquid water content (θ_w) and storage capacity of the melting snowpack. The combination of upward looking ground-penetrating radar and conventional snow height sensors enable continuous, nondestructive determinations of θ_w in natural snow covers from first surficial wetting until shortly before melt out. We analyze diurnal and seasonal cycles of θ_w for 4 years in a flat study site and for three melt seasons on slopes and evaluate model simulations for two different water transport schemes in the snow cover model SNOWPACK. Observed maximum increases in θ_w during a day are below 1.7 vol % (90th percentile) at the flat site. Concerning seasonal characteristics of θ_w, less than 10% of recorded data exceed 5 vol % at the flat site and 3.5 vol % at slopes. Both water transport schemes in SNOWPACK underestimate maximum θ_w at the flat site systematically for all observed melt seasons, while simulated θ_w maxima on slopes are accurate. Implementing observed changes in θ_w per day in outflow predictions increases model performance toward higher agreement with lysimeter measurements. Hence, continuously monitoring θ_w improves our understanding of liquid water percolation and retention in snow, which is highly relevant for several aspects of the cryosphere such as avalanche formation, catchment hydrology, and ice sheet mass balances.

1. Introduction

The presence of liquid water in snow and firn is highly relevant to cryospheric processes and monitoring systems recording their changes. The infiltration of liquid water into snow alters snowpack stratigraphy, microstructure [*Colbeck*, 1997], and snowpack stability [e.g., *Conway and Raymond*, 1993]. Consequently, avalanche forecasts, for example, rely on accurate determination of the temporal evolution of the bulk volumetric liquid water content (θ_w) and percolation depths. *Baggi and Schweizer* [2009] and *Mitterer et al.* [2011a] thoroughly summarize the formation of wet snow avalanches. A change in θ_w influences the onset of melt water runoff from the snowpack, which is important for flood and reservoir management [e.g., *Jones et al.*, 1983; *Kattelmann and Dozier*, 1999]. In addition, the initiation of liquid water percolation through the snow cover highly influences soil water contents and correspondingly soil ecosystems [*Maurer and Bowling*, 2014].

With regard to remote sensing, liquid water in snow alters the data retrieved by microwave (C/X bands) [e.g., *Shi and Dozier*, 1995] to infrared ranges [*Gupta et al.*, 2005]. This circumstance allows to monitor the extent of melt for large snow-covered areas [e.g., *Nagler and Rott*, 2000]. For instance, over the last decade several observational records in extent of surface melt for the Greenland ice sheet have been detected utilizing such data [e.g., *Steffen et al.*, 2004; *Tedesco et al.*, 2013]. However, the percolation depth of surface melt events into the snowpack cannot be determined from remote sensing data. As a consequence, quantification of melt volumes and percolation depend primarily on model predictions.

To date, model results on liquid water percolation in snow have almost exclusively been evaluated for snowpack outflow [e.g., *Essery et al.*, 2013; *Wever et al.*, 2014]. However, *Essery et al.* [2013] demonstrate that implementing storage of liquid water within the snow cover is important for improving model performance. For firn, *Harper et al.* [2012] and *Gascon et al.* [2014] state that observations of vertical infiltration are lacking. Without evaluation against observations, it remains unclear whether models accurately reproduce mass

transport and heat advection through refreezing. Comparing monitored diurnal and seasonal changes of θ_w in snow on slopes and flat sites with model simulations enables identification of current deficits in model parameterizations.

One commonly applied model to describe liquid water percolation in snow and firn is a bucket approach [e.g., *Munneke et al.*, 2014; *Wever et al.*, 2014]. Here each individual snow or firn layer is filled to its storage capacity before it drains water to the next layer below. The main parameter for each modeled layer is the maximum holding capacity or irreducible water content (θ_{wi}). *Coleou and Lesaffre* [1998] and *Schneider and Jansson* [2004] performed cold-lab experiments to determine the irreducible water content for several snow samples with varying grain sizes and densities. Numerous studies rely on these empirical results for modeling water transport in snow [e.g., *Gascon et al.*, 2014; *van Pelt et al.*, 2014]. In accumulation areas of polar regions, this bucket approach, which considers percolation as homogeneous flow process cannot reproduce observed conditions [*Gascon et al.*, 2014]. Also, *Wever et al.* [2014] show that the bucket approach is inappropriate to model outflow with a high temporal resolution, i.e., for timescales of less than 6 h. To improve percolation simulations in snow within the one-dimensional snow cover model SNOWPACK [*Bartelt and Lehning*, 2002; *Lehning et al.*, 2002a, 2002b], *Wever et al.* [2014] introduce a solver for Richards equation (RE) to model water percolation in snow. This water transport scheme provides more accurate results on snowpack outflow on a subdaily temporal resolution [*Wever et al.*, 2014].

Continuous nondestructive observations are indispensable to evaluate model performances with regard to, both, the temporal evolution of θ_w and the infiltration progress of liquid water in snow. Upward looking ground-penetrating radar (upGPR) systems in combination with conventional snow height sensors provide such data [e.g., *Heilig et al.*, 2010; *Mitterer et al.*, 2011b; *Schmid et al.*, 2014].

The aim of this paper is to present continuous data sets, over several consecutive melt seasons on diurnal and seasonal changes of θ_w in snow on slopes and at a flat study site. Since destructive manual observations provide only temporal snapshots and can be influenced by spatial differences from one observation to the other, they are inappropriate to evaluate model performance. In this study, we use upGPR data to derive θ_w and changes in storage capacity in undisturbed natural snow covers. Based on these multiyear observations, we describe characteristics of diurnal and seasonal behavior of θ_w, analyze differences between slopes and flat sites, and evaluate two different water transport schemes in SNOWPACK. In addition, we determine accuracies of outflow simulations for various model approaches ranging from a simple temperature index method to the incorporation of RE in SNOWPACK. In addition, we integrate characteristics of diurnal changes of water retention, based on radar, into two outflow simulations and analyze their analogy to measured outflow sums.

2. Methods

2.1. Test Sites and Radar Instruments

We combined data from three different test sites for this study. Two upGPR systems were installed in slopes and one at the flat study site Weissfluhjoch (WFJ) above Davos, Switzerland [*Mitterer et al.*, 2011b] (2540 m above sea level (asl), 46.83°N, 9.81°E; dual-frequency 600/1600 MHz antennas; see *Schmid et al.* [2014] for more radar details). The test site Dorfberg (DFB) is situated in a southeast facing slope inclined by 22° above Davos as well [*Schmid et al.*, 2012] (2240 m asl, 46.82°N, 9.83°E). This site is equipped with a 900 MHz single-frequency system manufactured by IDS Ingegneria dei Sistemi, Pisa, Italy. The second slope site, Bogus Basin (BB) [*Heilig et al.*, 2012] (2105 m asl, 43.76°N, −116.09°W), is located next to the ski resort Bogus Basin, Idaho, USA. The upGPR was also installed within a 22° inclined southeast facing slope. This site was equipped with an 800 MHz single-frequency system manufactured by MALA Geoscience, Sweden.

All upGPR systems measured periodically from every 3 h to every half hour during the day. Nocturnal measurements had to be spaced by up to 6 h due to power constraints at the two slope sites. Both slope sites were solely run by solar power and batteries. All three deployed upGPR systems were vertically moved up and down beneath the ground surface (from 0.12 to 0.18 m uplift distance) twice during each radar measurement. *Heilig et al.* [2009, 2010] describe in detail the benefits for data processing of vertically moving upGPR antennas. The data processing for all radar records was similar to *Schmid et al.* [2014]. Snow surfaces in the resulting radar images were determined using the "semi-automated picking algorithm" described in *Schmid et al.* [2014].

The test site WFJ is equipped with automatic weather stations (AWSs) with numerous sensors to record meteorological and snow cover properties [*Marty and Meister*, 2012; *Mitterer et al.*, 2011b]. At DFB, we installed two ultrasonic range finders directly above the upGPR system on a wooden frame with a 12 cm thick cross

beam on top. This cross beam was almost constantly detectable throughout the whole season acting as target reflection. On both slopes, the ultrasonic range finders were installed in slope-normal direction, hence measuring the snow thickness (DS). At BB, it was impossible to mount the ultrasonics right above the upGPR location due to time constraints with an early winter snow cover. The snow depth sensor was installed about 5 m in horizontal distance from the radar antennas with the possible risk of variable melt out between the two locations.

Accompanying to upGPR and AWS data, we performed conventional snow pit measurements conducted in accordance to *Fierz et al.* [2009]. In the snow pits, we recorded the relative dielectric permittivity using the Denoth capacity plate [*Denoth*, 1994]. During wet snow conditions, the combination of recorded density and permittivity values from the Denoth capacity plate allows calculating θ_w by using empirical relationships [e.g., *Denoth*, 1994]. Occasionally, the Finnish Snow Fork was used to determine θ_w, especially in 2013. *Techel and Pielmeier* [2011] describe the functionality of this device in more detail.

2.2. Derivation of Liquid Water Content

Schmid et al. [2014] describe the methodology to derive θ_w values and dry snow density from radar-recorded two-way travel times (τ) and measured snow depth. For this study, we just apply the physically based three-phase mixing formulation published by, e.g., *Roth et al.* [1990] or *Wilhelms* [2005]:

$$\varepsilon_s^\beta = \varepsilon_i^\beta \theta_i + \varepsilon_a^\beta \theta_a + \varepsilon_w^\beta \theta_w, \tag{1}$$

with $\theta_a + \theta_i + \theta_w = 1$, the contributing volume fractions of snow (air a, ice i, and water w); the exponent β, which has to be adjusted in accordance to medium properties; and ε, the respective dielectric permittivities with the mixing permittivity ε_s of snow (s) [e.g., *Mitterer et al.*, 2011b].

However, during wet snow conditions the system of equations is underdetermined for the available instruments in the field. It is impossible to independently discriminate θ_i, θ_a, and θ_w. Continuous upward looking radar data enable monitoring of the bulk density ρ_s for dry snow ($\theta_w = 0$). To compensate for the unknown ice volume fraction in wet snow, we assume that the dry snow density remains constant after initial wetting. Following *Schmid et al.* [2014], we determine the average dry snow density using 100 consecutive measurements right before the first surface wetting is recognizable in the radar data. Utilizing $\varepsilon_w = 87.9$, $\varepsilon_i = 3.18$, $\varepsilon_a = 1$, and $\beta = 0.5$ [e.g., *Mitterer et al.*, 2011b; *Schmid et al.*, 2014], we now can solve equation (1). To analyze uncertainties in θ_w arising from the assumption of $\theta_i = \text{const}$, we use an empirically determined equation to solve for θ_w, taking measured densities in wet snow into account [*Denoth*, 1994]:

$$\varepsilon_s = 1 + c_1 \rho_s + c_2 \rho_s^2 + c_3 \theta_w + c_4 \theta_w^2, \tag{2}$$

with $c_1 = 1.92 \times 10^{-3}$, $c_2 = 4.4 \times 10^{-7}$, $c_3 = 18.7$, and $c_4 = 45$. For ρ_s, we use bulk densities measured in snow pits. For the time periods in between pit observations (from 2 to 40 days, variable for site and melt season), we linearly interpolate bulk density for each radar recording.

Maximum daily increases of θ_w ($\Delta\theta_{w-\max}$) are determined by subtracting θ_w from the 6:00 h measurement and taking the maximum value per day. At 6:00 h usually a minimum in diurnal θ_w is reached.

To determine the mass of liquid water m_w, we have to estimate the imaged radar volume for each measurement. Since changes in ε_s alter the radar wave refraction at permittivity transitions, the scanned volume depends on DS and ε_s. For simplicity, we consider ε_s to be homogeneous within the snowpack; i.e., just one refraction from air to snow is accounted for. In addition, the opening angle of the antennas is given by the manufacturers as 45°. Thus, we can determine the illuminated surface area (A_{surf}) and radar-imaged volume (V_{cone}) in snow for each individual measurement. This is converted to a cylinder volume (V_{cyl}) with base area A_{surf} and the height DS. Since the imaged volume is a truncated cone with variable opening angles, we extend V_{cone} to V_{cyl} to enable normalization of m_w per square meter surface area ($\hat{m}_w$). The mass of water for each individual radar measurement given per 1 m^2 surface area calculates to $\hat{m}_w = f_{\text{vol}} \theta_w \rho_w V_{\text{cone}} A_{\text{surf}}^{-1}$, with $f_{\text{vol}} = \frac{V_{\text{cyl}}}{V_{\text{cone}}}$. The mass increase over 24 h $\hat{m}_{\text{wi}} = \sum \frac{d\hat{m}_w}{dt}$ results in the mass of irreducible water being stored within the snowpack for this time period. Values of $\hat{m}_w$ are only calculated for equation (1).

At the slope site DFB, we can determine DS independently from data recorded by the ultrasonic sensors. Due to the fact that the cross beam is at a constant distance above the antennas and the dielectric permittivity of air is $\varepsilon_a = 1$, we simply use the measured two-way travel time of the snow surface to determine DS right above the antennas.

2.3. Snowpack Outflow

Liquid water outflow was measured at the test site WFJ with a 5 m^2 lysimeter [*Wever et al.*, 2014]. AWS data on radiation, precipitation, temperature, wind, and humidity were used for diurnal and seasonal estimates of melt rates and to simulate outflow. We compare outflow simulations of five approaches, which take into account the surface energy fluxes (M_S, M_{SR}, M_{SB}, M_{MB}, and M_{RE}; for detailed description see the notation section and the following subsections) and a simple temperature index method (M_D, with radar-determined corrections for diurnal changes in residual water M_{DR}) with lysimeter measurements.

2.3.1. Determination of Snow Melt From Meteorological Parameters

Radiation data were recorded by three different automatic weather stations (AWSs) in close proximity to the upGPR locations. Remaining surface energy fluxes (sensible and latent heat fluxes) are simulated using the one-dimensional snow cover model SNOWPACK [*Bartelt and Lehning*, 2002; *Lehning et al.*, 2002a, 2002b, 2002c]. These turbulent fluxes are simulated using a bulk transfer formulation, in which fluxes are expressed as differences between the snow surface and the height of the measuring sensor. In addition, we take atmospheric stability into account using a common form of the Monin-Obukhov bulk formulation [*Lehning et al.*, 2002c] and use a roughness length of 0.002 m [*Stössel et al.*, 2010]. Heat advected to the snow surface by liquid precipitation is considered for the determination of the surface energy fluxes, but ground heat flux is not taken into account. At the snow surface, Neumann boundary conditions are applied for solving the heat advection equation. SNOWPACK adds new layers for every snowfall resulting in a typical layer thickness of 2 cm in the simulations (depending on settling rates and element merging). The mechanisms for new snow layers and layer merging are discussed in *Wever et al.* [2014].

As alternative to more sophisticated, more data requiring energy balance approaches, simple temperature index methods are in use to solve for snow and ice melt [e.g., *De Michele et al.*, 2013; *Juen et al.*, 2014]. Temperature index methods use a daily mean of positive ($T_A > 0°C$) air temperature records (T_{avg}) and convert average temperature to melt by a degree-day factor (DDF) [e.g., *Braithwaite*, 1995]. For the test site WFJ, a 28 year long data record resulted in an average of 4.2 for the degree-day factor [*de Quervain*, 1979]. This leads to a daily melt for the temperature index model M_D (kg $m^{-2}d^{-1}$) of

$$M_D = 4.2T_{avg}. \tag{3}$$

Melt rates resulting from the net energy per day M_S (kg m^{-2} d^{-1}) can be expressed as [*King et al.*, 2008]:

$$M_S = \left(\frac{dH}{dt} + \int_0^{DS} \frac{dQ_c(z,t)}{dt} dz \right) \frac{1}{L_i}. \tag{4}$$

While $\frac{dH}{dt}$ is defined as the sum of energy fluxes scaled to the respective time steps (24 h), $Q_c(z,t) = -k_{eff}\frac{\partial T}{\partial z}$ is the heat flux defined as thermal conductivity (k_{eff}) times the temperature gradient [*Luce and Tarboton*, 2010]. L_i represents the latent heat of fusion of ice (3.34×10^5 J kg^{-1}). For k_{eff}, we used an empirically determined density relation by *Calonne et al.* [2011].

2.3.2. Simulation of Snowpack Outflow

From determined melt rates, it is possible to simulate diurnal and seasonal outflow from the snowpack. At WFJ, outflow is modeled for a whole day again to a 6:00 h reference and normalized for an area of 1 m^2. Lysimeter outflows are normalized for the same area and summed for 24 h. The liquid water retention is not considered in the formulation of the melt rate (equation (4)). Equations (3) and (4) can be corrected for diurnal changes in θ_w through subtraction of radar-determined $\hat{m}_{wi}$ to

$$M_{DR} = 4.2T_{avg} - \hat{m}_{wi} \tag{5}$$

$$M_{SR} = \left(\frac{dH}{dt} + \int_0^{DS} \frac{dQ_c(z,t)}{dt} dz \right) \frac{1}{L_i} - \hat{m}_{wi}. \tag{6}$$

The term $\hat{m}_{wi}$ is adjusted to $\hat{m}_{wi} = 0$ for days (24 h) when $\sum \frac{dDS}{dt} > 0$; i.e., the total snow thickness increases. For such cases, the observed decrease in θ_w is related to the increase in snow height rather than outflow. Furthermore, maximum θ_w values are set to remain within the pendular regime (8 vol %) [*Fierz et al.*, 2009] to minimize influences of erroneous radar-determined θ_w variations from one day to another.

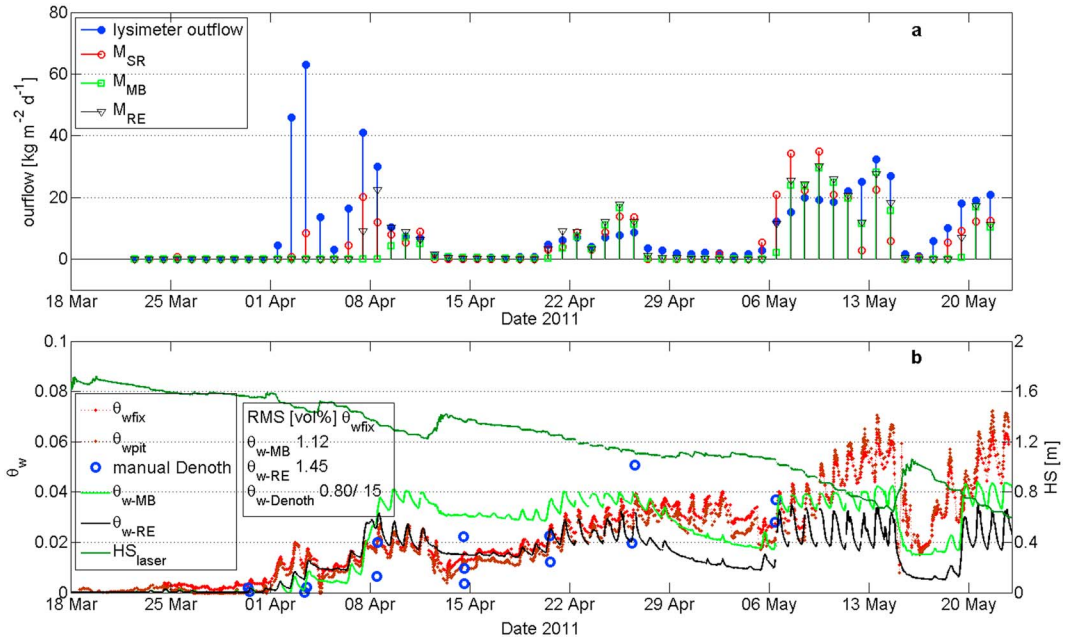

Figure 1. (a) Diurnal melt rates for the flat site WFJ in spring 2011 using upGPR measurements corrected for $\hat{m}_{wi}$ (M_{SR} = red circles), SNOWPACK with multilayer bucket model (M_{MB} = green squares), and with Richards equation (M_{RE} = black triangles), along with measured lysimeter outflow (blue dots). (b) Seasonal characteristics for θ_w determined from radar data (red) with uncertainty range (brown), modeled with M_{MB} (θ_{w-MB} = green line), with M_{RE} (θ_{w-RE} = black line), and manual Denoth measurements (blue circles), observed snow heights (HS_{laser} = dark green curve) by laser gauge. The absolute deviations in vol % to radar θ_w are presented in the RMS box; second number describes sample size.

Including an empirical relation of snow density to gravitational irreducible liquid water content (θ_{mi}) [*Schneider and Jansson*, 2004] leads to a simple one-layer bucket approach (SB) for the whole snow cover. Again, we use diurnal averaged densities for the determination of θ_{mi}. This leads to a reduced outflow until $\theta_w = \theta_{wi}$; i.e., the maximum holding capacity of the snow cover is reached. The outflow model utilizing the bucket approach is referred to as M_{SB}. Such a bucket approach is widely used in current literature to estimate water transport for studies in polar as well as alpine regions [e.g., *Munneke et al.*, 2014; *van Pelt et al.*, 2014; *Wever et al.*, 2014].

In addition, we use 15 min outputs from SNOWPACK for bulk liquid water content and simulated outflow per square meter. For the flat site WFJ, SNOWPACK is snow height driven with either using (1) a multilayer bucket approach (MB) [e.g., *Wever et al.*, 2014] or (2) Richards equation (RE) with the Yamaguchi water retention curve [*Yamaguchi et al.*, 2012] described in *Wever et al.* [2015].

Diurnal outflow sums are referred to as M_{MB} for the multilayer bucket model and M_{RE} for SNOWPACK with incorporation of Richards equation for water percolation processes. For the slope simulations, we use DS measured directly above the radars for the DFB site and measurements from an AWS being located about 30 m higher in elevation for the BB site. Additional parameters to run SNOWPACK are interpolated for the slope locations from available AWS data.

3. Data Review

Both lysimeter measurements and upGPR data required data inspection before further analysis. Radar-determined θ_w and modeled θ_w cycles, manually determined θ_w snapshots, measured DS, measured diurnal outflow rates, and simulated outflow rates are presented in Figures 1–7. Figures 1a, 2a, 3a, and 4a present outflow measurements from the lysimeter (blue) in comparison with modeled outflow values for radar-corrected M_S in equation (6) (red circles), daily sums of outflow from the one-dimensional model SNOWPACK utilizing the multilayer bucket approach (green squares), and outflow sums from SNOWPACK utilizing Richards equation to assess liquid water percolation (black triangles). Figures 1b, 2b, 3b, 4b, and 5–7 display the radar-determined seasonal cycles in θ_w (red), the determined uncertainty range utilizing

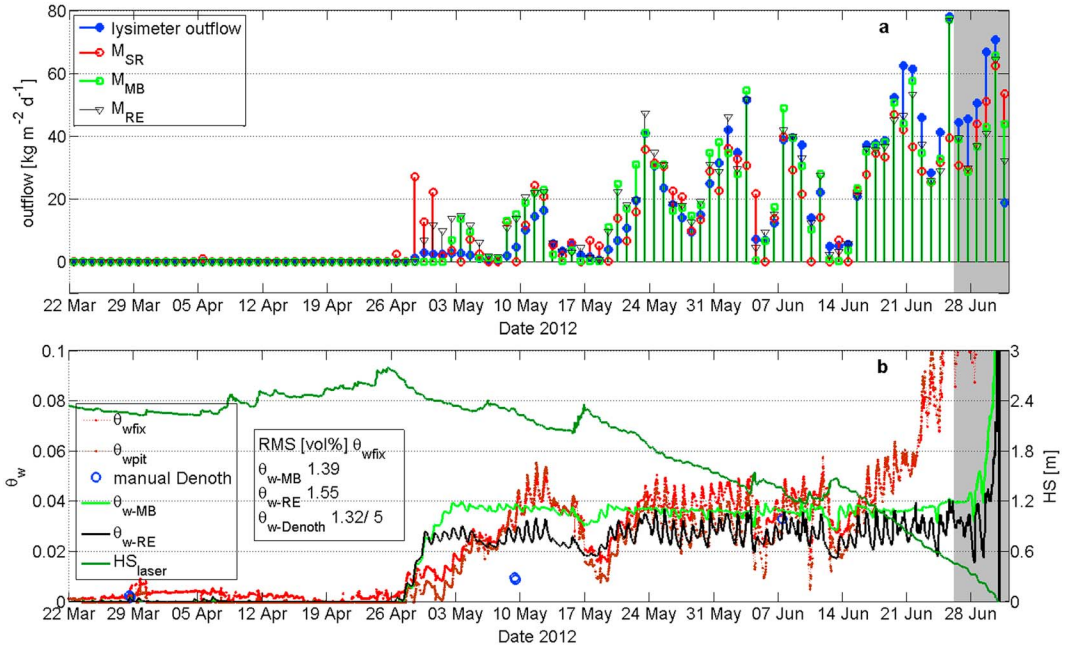

Figure 2. (a) Diurnal melt rates and (b) seasonal characteristics for θ_w for the flat site WFJ in spring 2012. The gray shaded period represents dates when upGPR data are not reliable; for other notations see Figure 1.

measured wet snow densities as described in equation (2) (brown), manual determinations of θ_w in snow pits using the Denoth capacity plate (blue circles), and Finnish Snow Fork (blue triangles) and model outputs from SNOWPACK utilizing the multilayer bucket approach (green) and Richards equation (black). In addition, we included values for root-mean-square (RMS) deviations to radar-derived θ_w from equation (1) in vol % for the manual measurements (plus number of observations) and SNOWPACK outputs. For comparison, we plotted measured DS (dark green) as additive information.

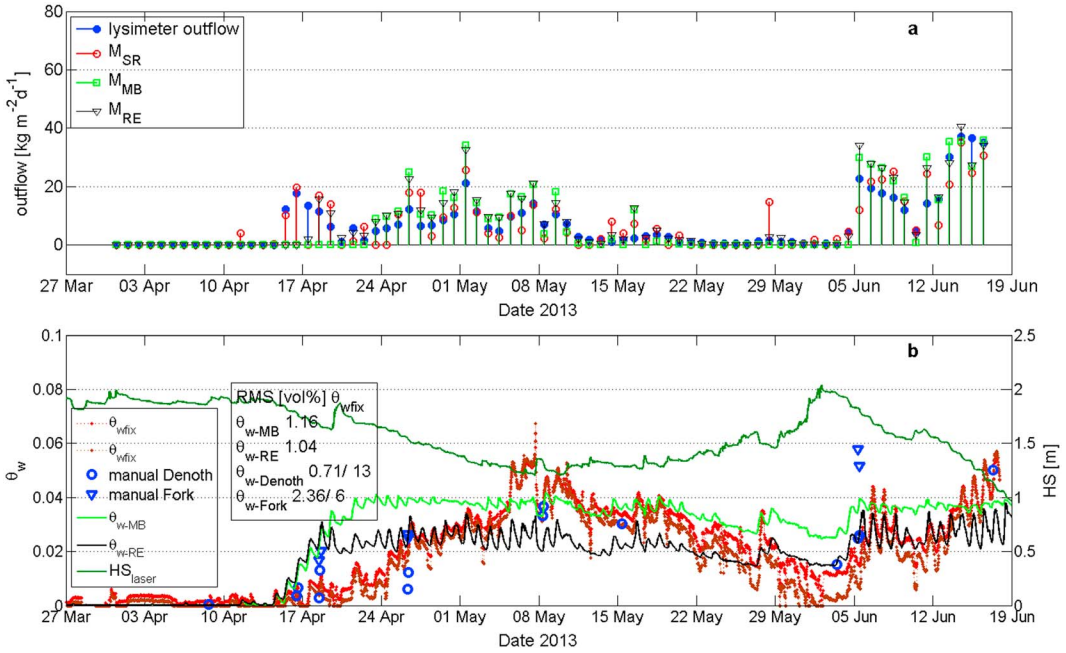

Figure 3. (a) Diurnal melt rates and (b) seasonal characteristics for θ_w for the flat site WFJ in spring 2013. Manual Finnish Snow Fork data are presented through blue triangles; for other notations see Figure 1.

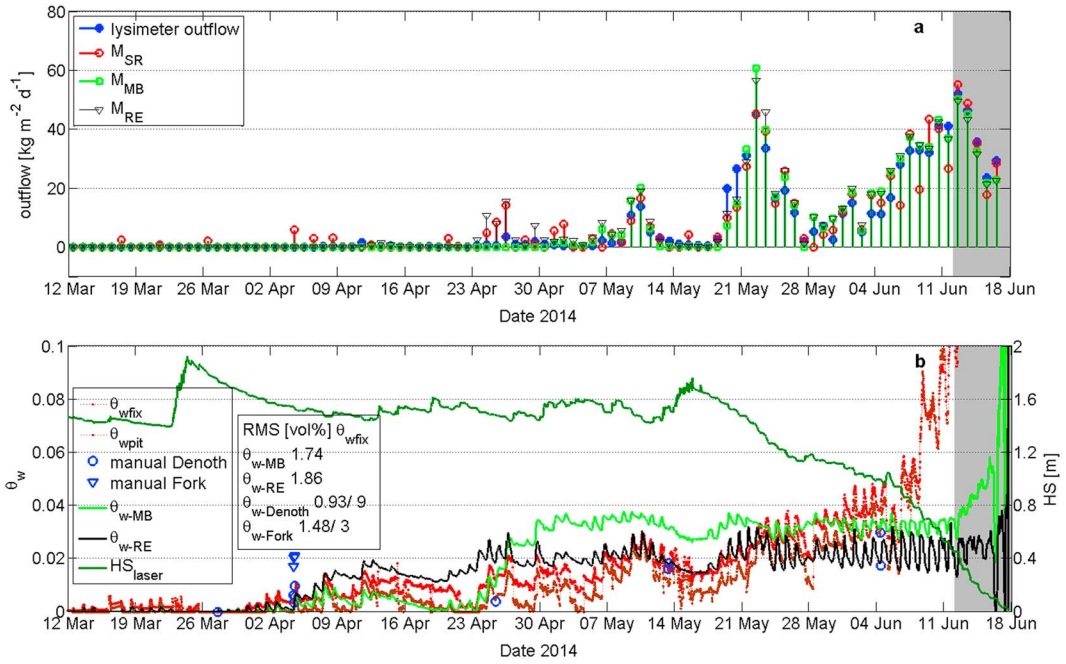

Figure 4. (a) Diurnal melt rates and (b) seasonal characteristics for θ_w for the flat site WFJ in spring 2014. The gray shaded period represents dates when upGPR data are not reliable; for other notations see Figures 1 and 3.

3.1. Lysimeter

The lysimeter location at the flat site WFJ is at approximately 30 m distance from the upGPR site [*Wever et al.*, 2014]. In spite of the lysimeter being surrounded by 0.6 m high metal boards, measurements can be influenced by lateral flow and, hence, may represent data for a much wider area than just 5 m^2. To check lysimeter data for reliability, we determined the mean density of the melted snow mass considering the snow height change per day ($\Delta DS = DS_{max} - DS_{min}$ per 24 h period) measured by the laser DS sensor together with lysimeter-measured runoff sums per day (LO) by $\rho_{lysi} = LO(\Delta DS)^{-1}$. The laser DS sensor is located about 26 m from the lysimeter. Maximum densities measured in snow pits were always below $\rho_s < 580$ kg m^{-3}. Hence, when $\rho_{lysi} > 580$ kg m^{-3}, we consider measured runoff to be not reliable for further analysis. We expect two reasons for mismatches between lysimeter data and laser data: (1) strong spatial differences in melt between the two locations and (2) lateral flow causing observed runoff at the lysimeter to be nonrepresentative for the measurement area of the lysimeter (5 m^2).

3.2. upGPR

In periods of strong snow melt, the upGPR at the flat site WFJ was affected by water inrushes. Since the radar antennas are installed beneath the ground surface, the antenna box can get flooded after soil saturation. As a consequence, the melt periods of the winter season 2010/2011 and 2012/2013 were not recorded in their full

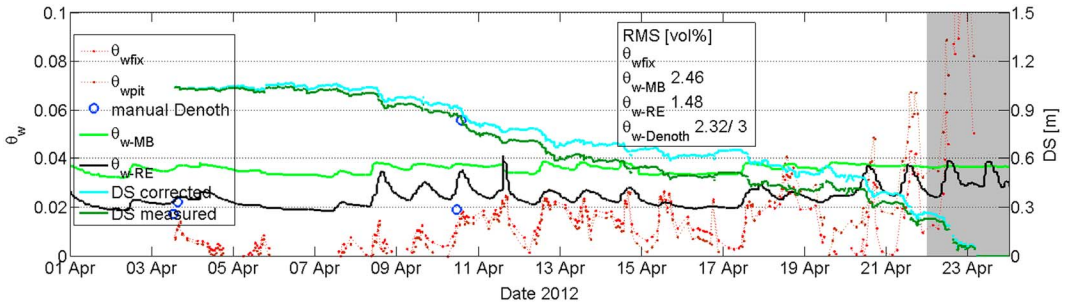

Figure 5. Seasonal characteristics for θ_w for the slope site BB in spring 2012. Assimilated DS data are presented (light blue curve) in addition. The gray shaded period represents dates when upGPR data are not reliable; for other notations see Figure 1.

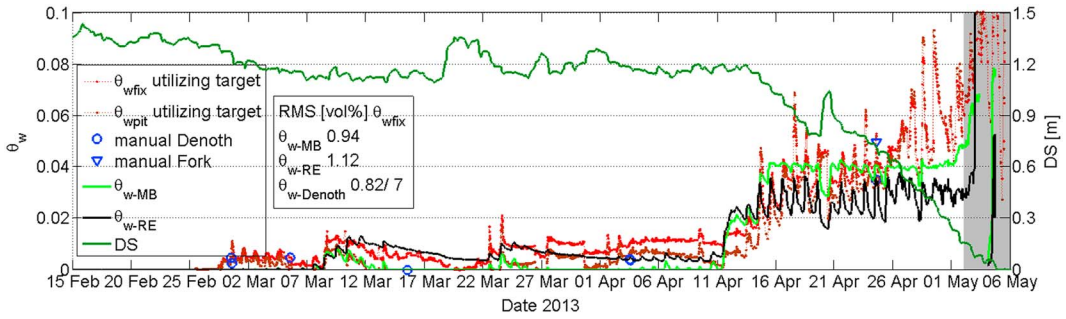

Figure 6. Seasonal characteristics for θ_w for the slope site DFB in spring 2013. The gray shaded period represents dates when upGPR data are not reliable; for other notations see Figure 1.

entirety. At 22 May 2011 and 17 June 2013, the radar stopped recording after water seeped into the antenna housing. With the help of water pumps and better water shielding, the melt seasons 2012 and 2014 at the flat site are presented until complete melt out. In periods of strong melt, which induce generation of surface roughness (concave furrows) and increase signal attenuation, we make use of the low-frequency part of the dual-frequency setup at WFJ. However, surface detection with the 600 MHz antennas is only possible until DS or the amplitude of surface features hit the resolution limits ($\lambda/2 = 0.19$ m in dry snow; $\lambda/2 \approx 0.15$ m in wet snow). For snow heights below 0.15–0.2 m signal interferences from the ground reflections, the interface air-snow beneath the snowpack and the snow surface occur for the 600 MHz system as well.

Larger spatial heterogeneities in DS than within the flat site WFJ require installation of DS sensors exactly above the GPR instruments to allow calculating θ_w or density.

Data for the slope site Bogus Basin are only present for April 2012. Due to technical constraints with the ultrasonic snow height sensors, radar-based melt observations started not before 3 April in 2012. Various melt and rain-on-snow events occurred already prior to this date, but melt was interrupted for 3 days with constant negative air temperatures before 3 April 2012. As being recognized after melt started, the slope site is largely heterogeneous in terms of incline and, hence, melt. During April 2012, offsets in snow probings at locations directly above the upGPR antennas and right underneath the ultrasonic sensor were strongly nonlinear. Accepting this nonlinearity would result in continuous increases in θ_w values with advancing melt out. To compensate for this offset, we corrected the snow depth at the ultrasonic sensor in accordance to measured offsets between ultrasonic and upGPR location (Figure 5, two different DS curves). We assumed a steady temporal trend in offset in between site visits and, hence, compensated the snow thickness above the radar in accordance to the trends in offsets in between snow probings.

At DFB in the winter season 2012–2013, two wooden boards were arranged above the radar antennas in 1–3 cm distance to each other. During strong melt, when both boards got wet, signal attenuation was very high and the target reflection response from above the snow surface strongly reduced. The installed ultrasonic depth rangers oscillated too strongly for usage as backup for the missing target signals. Hence, extreme values of this data set are of limited reliability especially for the peaks in melt (after 16 April 2013; Figure 6). In 2014, from 14 February until 20 February the upGPR hoisting mechanism at this site failed. The strong increases in θ_w for 16 February are not reliable. From 21 February on, everything worked normally and recorded radar data are of high-quality again.

4. Results and Discussion

4.1. Uncertainty Analysis for Observations

Schmid et al. [2014] describe several sources for errors in determining snowpack parameters (e.g., dry snow density, new snow sums, and total mass of accumulation) from radar wave speed in combination with externally measured snow height (here DS). The same problems occur for deriving θ_w from radar data and inverting for residual water content. The results are highly dependent on correct surface picks and the absence of spatial variability in snow height between radar and DS sensor location. Especially for low DS, shortly before melt out, variability between both locations can result in large errors. For instance, for DS = 0.4 m a spatial offset in snow height of ±0.05 m results in a relative variability of θ_w of ±30–35% depending on the bulk density. In addition, such periods usually reside in situations of water saturation of the ground and fairly large θ_w within

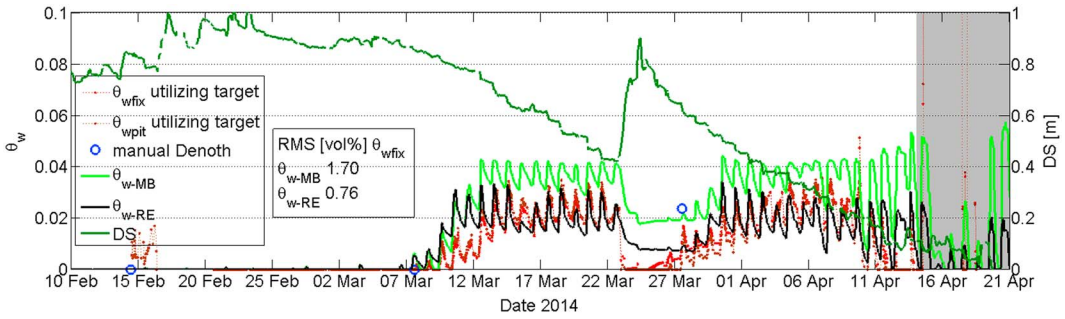

Figure 7. Seasonal characteristics for θ_w for the slope site DFB in spring 2014. The gray shaded period represents dates when upGPR data are not reliable; for other notations see Figures 1 and 3.

the snow cover. Hence, radar signals are strongly attenuated, the ground reflection changes with saturation stage during the day, the residual snowpack becomes patchy, and the snow surface may become very rough (concave furrows). Every single condition of the named combination of parameters is negatively influencing radar signal accuracy with the consequence that upGPR reaches its limits of accuracy. This is the reason for our definition of periods when radar measurements are of limited quality and reliability. We indicate such data in Figures 2 and 4–7 through gray shaded periods and in Tables 1 and 2, periods for which upGPR provides reliable data are labeled "corr."

Another dominant source of error can be spatial differences in meltwater percolation and liquid water outflow between the locations of radar and lysimeter. Since a significant amount of water is already transported through the snowpack via heterogeneous flow [e.g., *Pfeffer et al.*, 1991]—especially before stable wetting fronts have reached the ground—large differences in runoff amounts may occur over short distances. It is impossible to quantitatively assess these offsets in location. However, since both instruments (lysimeter and upGPR) integrate over a relatively large surface area (lysimeter 5 m^2; upGPR 2–8 m^2), spatial variability in melt water percolation is reduced to a certain degree.

Additional circumstances complicating the determination of bulk θ_w are small new snow accumulations on already wet snowpacks. Here radar reaches its resolution limits. Wet snow causes strong attenuation, especially for high-frequency systems, and vertical layer resolution depends on wavelength within the penetrated medium [e.g., *Daniels*, 2004]. However, snowfalls on wet snow covers cause only short-term inaccuracies of less than a few hours, since either further new snow improves detectability or settling and surface wetting quickly enable a clear surface signal response.

It is impossible to derive θ_w directly from upGPR data. Only ε_s is directly determined from the measured parameters τ and DS. We use the assumption that θ_i is constant after initial wetting to convert ε_s to θ_w. For the presented test sites and melt seasons, the empirically determined θ_w relation by *Denoth* [1994] (section 2.2) agrees fairly well with the θ_w values calculated with equation (1), and hence, the uncertainty in θ_w resulting from setting $\theta_i = const$ is rather low. The average deviation of θ_w at WFJ for results determined with equation (2) is 0.35 vol % (median: 0.35 vol %, 90th percentile: 0.74 vol %, max: 1.25 vol %—for "corr" periods).

Table 1. Cumulative Deviations for Measured Outflow in Comparison to Simulations[a]

Site Year	Outflow (kg m^{-2})	ΔM_S	ΔM_{SR}	ΔM_D	ΔM_{DR}	ΔM_{SB}	ΔM_{MB}	ΔM_{RE}
WFJ2011	309.1	−37.6	−26.9	−32.3	−18.4	−40.6	−70.2	−19.9
WFJ2012	631.3	114.4	32.1	33.5	−20.0	80.4	82.2	138.6
WFJ2012 corr	581.0	130.2	38.6	34.0	−27.7	95.2	96.0	152.2
WFJ2013	507.8	78.4	−4.3	−3.3	−59.3	41.5	40.6	103.9
WFJ2014	655.5	80.9	46.4	−28.2	−25.5	26.1	36.2	115.7
WFJ2014 corr	451.4	107.3	42.4	40.5	12.8	52.5	48.9	136.7
Average (%)		17.95	6.20	6.29	6.25	12.09	14.26	20.22

[a]Outflow represents sums of lysimeter measurements per observation period; the cumulative sums are calculated for model simulations subtracted by measurements per day in kg m^{-2}. For simulation abbreviations see the notation section.

Table 2. Differences Between Measured Outflow Per Day and Simulated Daily Outflow Presented Through Root-Mean-Square (RMS) Deviations in kg m^{-2}[a]

Site Year	M_S	M_{SR}	M_D	M_{DR}	M_{SB}	M_{MB}	M_{RE}
WFJ2011	4.62	5.42	3.85	4.55	4.62	4.90	4.25
WFJ2012	6.77	5.97	8.85	8.33	5.89	4.92	4.60
WFJ2012 corr	6.62	5.97	8.91	8.34	5.70	4.71	4.38
WFJ2013	3.94	4.68	4.57	5.21	4.74	5.69	5.13
WFJ2014	3.87	4.04	6.49	5.91	3.41	2.84	3.57
WFJ2014 corr	3.70	4.11	5.52	5.60	3.19	2.79	3.52
Average	4.72	5.05	5.71	5.93	4.56	4.52	4.32

[a]For simulation abbreviations see the notation section.

For the observed slopes, the average offset is 0.33 vol % (median: 0.39 vol %, 90th percentile: 0.75 vol %, max: 1.14 vol %—for "corr" periods).

For the spring seasons 2013 and 2014 at WFJ, GPS receivers were installed at the ground surface in a distance of 16 m to the upGPR system. While upGPR systems measure wave speed alternations within the overlying medium, ground-based GPS receivers record signal attenuation and by this allow determining θ_w within the overlying medium. Deviations of upGPR-determined θ_w with values derived from the GPS receivers are low with resulting root-mean-square errors of 0.4 to 0.7 vol % [*Schmid et al.*, 2015]. However, preconditions to derive θ_w from upGPR and GPS are exactly the same. Both systems assume a constant dry snow density, calculate dielectric permittivity with $\beta = 0.5$, and use measured DS from the nearby laser gauge. Interpreting the presented offsets, we claim that with the applied radar system and conversion scheme, it is possible to monitor diurnal and seasonal θ_w evolution in snow with an absolute accuracy of about 0.5 vol %.

There are several other possible—mostly empirically based—conversion schemes in literature [e.g., see *Heilig et al.*, 2009]. The three-phase mixing formula (equation (1)) is the most physically based relation without site-specific, empirically determined constants apart from the exponent. From DS measured directly above the radar antennas and ρ_s in pits, we analyzed the variability of the exponent β for dry snow conditions as well. For all winter seasons at the WFJ site, an average value of $\beta = 0.5$ with a standard deviation of 0.1 is determined ($N = 14$ samples). Variability in DS and ρ_s was too large within the slope sites to include them into this analysis. On the one hand, this result proves the statement by *Roth et al.* [1990] to use $\beta = 0.5$ for randomly stratified media. On the other hand, the high standard deviation shows that such an analysis strongly depends on accuracies and low spatial variabilities. In addition, since field measurements of θ_w with, e.g., the calorimetry method is hardly possible, no validation data for β in wet snow conditions are available. We have to assume that β does not vary with θ_w.

To compare outflow recorded by a 5 m^2 lysimeter with predicted outflow by several modeling approaches, we neglect those diurnal outflow sums, which cannot be reproduced by observed changes in DS and reasonable values of ρ_s. We attribute such large outflow sums to lateral flow. Such a correction for lateral flow disregards settling of the snow cover, which, in addition, would decrease ΔHS and consequently increase ρ_{lysi}. Furthermore, the threshold of $\rho_s \leq 580$ kg m^{-3} for possible snow densities is a conservative value. No conventional measurement of the bulk density reached such a high value. For each melt season at the WFJ several days (one to five depending on the individual season) of runoff were removed from analyses. Prominent examples for lateral flow conditions or high spatial variability within the test site are observable between 2 and 4 April 2011, from 6 to 8 April 2011 (Figure 1), and on 25 June 2012 (Figure 2). For all these dates the total snow height was larger than the height of the metal boards at the lysimeter and determined positive energy fluxes are not sufficient to melt the amount of runoff per square meter being recorded by the lysimeter (Figures 1 and 2).

4.2. Diurnal Increases in Volumetric Liquid Water Content

4.2.1. Radar-Determined Diurnal Increases

Figures 8a and 8b present statistics for $\Delta\theta_{w-max}$ determined with respect to the value recorded at 6:00 h in the morning each day for all sites and observed melt seasons. Maximum diurnal increases of liquid water at the flat site show a median value of 0.4–0.7 vol % (red lines in Figures 8a and 8b). In 75% of all days, the maximum diurnal increase in θ_w is less than about 1 vol %. Regarding the 90th percentile determined for the flat site, $\Delta\theta_{w-max}$ is below 1.7 vol % for all four observed melt seasons.

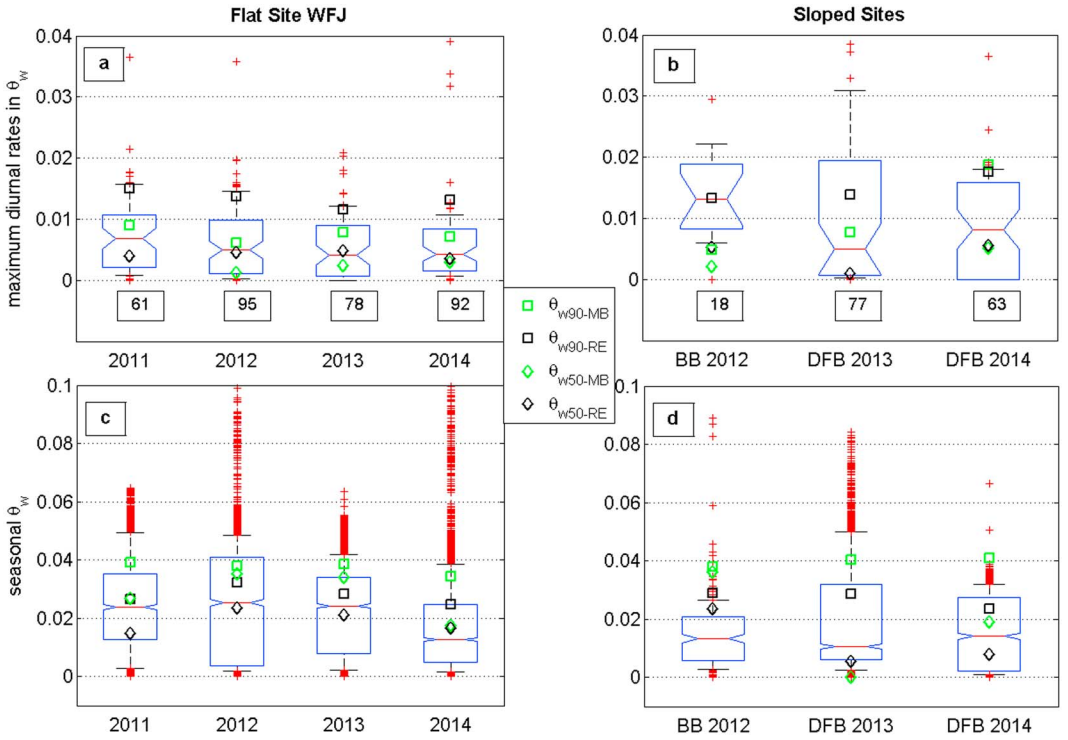

Figure 8. (a, b) Diurnal and (c, d) seasonal behavior of θ_w in snow at the observed sloped and flat sites and melt seasons. Values of θ_w are determined only for periods when radar can provide reliable data ("corr") while utilizing equation (1) in section 2.2. The red horizontal lines within the boxes represent the median in $\Delta\theta_{w-\max}$ (Figures 8a and 8b) and θ_w (Figures 8c and 8d), the boxes frame the interquartile range and the whiskers display the 10th respectively the 90th percentile. Outliers are presented through red crosses. All values are given in volumetric content per total volume. Green and black squares in all plots display 90th percentiles of predicted θ_w from SNOWPACK using a multilayer bucket approach (MB) and Richards equation (RE). The diamonds with the same color code represent median values of the respective model approach.

For the observed southeast facing slopes, values of $\Delta\theta_{w-\max}$ exceed the observations at the flat site. On slopes, the median values are about 0.5–1.3 vol % (Figure 8b). The upper quartiles in $\Delta\theta_{w-\max}$ are 2 vol % and thus approximately twice as large as at the flat site. The 90th percentiles show that only during the melt season in 2014, the value is below 2 vol % for $\Delta\theta_{w-\max}$. We cannot make any firm conclusions on differences in extreme values between flat sites and slopes since the Bogus site is situated in a different geographic and climatic region and during the melt season 2013 at the DFB site the setup caused problems. Just regarding the reliable data set of 2014 shows that even on slopes values of $\Delta\theta_{w-\max}$ are below 2 vol %. The hardly overlapping notches in Figure 8b suggest that the three seasons were different. Regarding the four consecutive melt seasons at the flat site WFJ (Figure 8a), the notches always overlap and the median for all seasons is fairly similar. The numbers below the box plots in Figures 8a and 8b display the sample sizes equivalent to the duration of the respective observed melt periods in days.

Our results suggest that regardless of variations in snow height and air temperature, a diurnal increase in θ_w larger than 2 vol % very rarely occurs and is limited to a few melt events at the very end of each snow season and possibly rain-on-snow events. However, during the presented melt periods, we did not observe rain-on-snow events. The maximum diurnal increase of 1.7–2 vol % certainly can be exceeded through strong rain events, especially when a large amount of latent heat is released within the snowpack. Such events are more common in coastal precipitation regimes than for the here observed rather continental climates.

4.2.2. Model Performance Evaluation for Observed Diurnal Increases in θ_w

Accuracies of the predictions of $\Delta\theta_{w-\max}$ in SNOWPACK are very high for the RE approach. Regarding the 4 years at WFJ and the one reliable observation period at DFB in spring 2014, it appears that RE in SNOWPACK simulates extreme values and medians in accordance with the radar data (Figures 8a and 8b). While outputs for the bucket approach at DFB 2014 are fairly equal to RE, large deviations occur for WFJ. Especially extreme

values are underestimated at the flat site with the consequence of a less accurate prediction of diurnal dynamics in θ_w for the bucket approach (see, e.g., Figure 2).

4.3. Seasonal Cycles in θ_w

4.3.1. Observed Seasonal Cycles in θ_w

In Figures 1b, 2b, 3b, 4b, and 5–7, we present manual observations of θ_w in snow pits, which are averaged for the bulk snow cover. RMS deviations in vol % are added to the respective plots when the sample size of RMS values is larger than 2. Generally, manually conducted θ_w measurements utilizing the Denoth capacity plate match radar-determined values with a mean absolute deviation of 0.7–0.9 vol % to the radar-determined observations. The larger discrepancies in 2012 for both the flat field and the slope observations can be explained by very low sample numbers and single outliers. For the very few Snow Fork results, we obtain a significantly larger deviation.

Figures 8c and 8d display the seasonal statistics for all sites and melt seasons. Again only periods of reliable radar data ("corr" periods) are included. The data show that at the WFJ site, the median bulk liquid water content (red horizontal lines) is about 2.5 vol % for the first three melt seasons. Only for the spring season 2014, the median θ_w is significantly lower at 1.2 vol %, mainly due to the long melt season with frequent snowfalls. For every observed melt period at WFJ, about 75% of θ_w values are below 4 vol %. In 2013 and 2014 even 90% of all values do not exceed 4 vol %. Regarding slope sites, a similar picture appears, but all median values are below 1–1.5 vol % and the upper quartile for all three boxes is at about 2–3 vol %. Spring 2013 at the DFB site is considered as exemption due to radar setup difficulties for periods of large θ_w (see section 3). The skewness in data toward larger θ_w is an indicator for these difficulties. In general, one explanation for the significant lower median values in θ_w on slopes can be lateral flow, which certainly occurs in sloping snowpacks and routes water laterally downward [*Eiriksson et al.*, 2013].

4.3.2. Model Performance Evaluation for Observed Seasonal Increases in θ_w

For the flat site WFJ, both SNOWPACK approaches (MB and RE) deviate from radar-determined θ_w (in RMS values) by more than 1 vol % for the observed "corr" periods (Figures 1b, 2b, 3b, and 4b). Constantly, both model approaches always predict a very fast increase in θ_w as soon as significant energy input reached the site. As soon as the lysimeter detected two consecutive days of liquid water outflow (Figures 1a, 2a, 3a, and 4a), both models surpass radar-determined θ_w. Predicted θ_w quickly converges to about 4 vol % for the multilayer bucket model and to 2–3 vol % for the RE approach. The simulated values remain at such high levels until new snow accumulations or refreeezing conditions slightly reduce θ_w (e.g., 1 June 2013, Figure 3b). For the flat site WFJ, deviations expressed by RMS values are usually larger for RE-predicted θ_w than for the bucket approach. Only in 2013, the RE approach in SNOWPACK simulates θ_w slightly more accurately than the bucket model.

For the slope sites, deviations between model outputs and observations have to be considered specifically for each season and site. Whether the large values of θ_w of 2–4 vol % modeled at BB in Figure 5 before April are reliable or not cannot be answered with the present data set. The upGPR data indicate much lower θ_w in early April 2012 with a distinct increase by 10 April 2012. At the slope site DFB in spring 2013 (Figure 6), $\theta_{w-\mathrm{RE}}$ follows observed θ_w accurately until 16 April 2013, while the MB approach underestimates θ_w significantly. The lower RMS value for the MB approach in Figure 6 is the result of the very variable and large radar-determined θ_w records after 16 April 2013. As mentioned above, upGPR has a reduced reliability for this period. Considering RMS values only for the period before 16 April results in deviations of only 0.64 vol % for the RE and 0.87 vol % for the MB approach. In 2014 at DFB, we observe again a very accurate prediction of the RE approach in SNOWPACK for θ_w. Here RMS values clearly indicate the more accurate modeling with the RE approach in comparison to a multilayer bucket model.

In Figures 8c and 8d, we included 90th percentiles of predicted θ_w of both water transport schemes in SNOWPACK. The multilayer bucket model, which is based on results by *Coleou and Lesaffre* [1998], shows a very homogeneous 90th percentile of θ_w at or slightly below 4 vol % for all slopes as well as the flat site. It strikes that on slopes the 90th percentiles of modeled and radar-determined θ_w match fairly well, while at the flat study site-modeled maximum values are consistently surpassed by observations for all years. For instance, in spring 2012 at WFJ, the 90th percentile of the bucket model is below the upper quartile of observations. Underestimations of the model are not only limited to the very end of each season during melt out (Figure 2b). Especially for this spring season at WFJ, upGPR data demonstrate that empirically determined maximum holding capacities for homogeneous snow samples implemented in multilayer bucket models are not representative for heterogeneous snowpacks with distinct layering. Within a flat site, water percolation is often obstructed by

the presence of capillary barriers or crusts such that the bulk liquid water content increases [e.g., *Waldner et al.*, 2004]. The 90th percentiles from the RE approach underrepresent the observed values even more significantly than the MB outputs in SNOWPACK. Maximum RE simulations (90th percentiles) are within a range of 50–75% of observation data at the flat site. On slopes, however, RE matches radar-determined θ_w accurately except at the very end of each melt period. Results for BB in 2012 are exemptions and related to the very short observation period and difficulties in measuring DS within the slope.

Mismatches in the increase of θ_w during early spring between model approaches and radar-determined values at the flat site are a consequence of the lacking scheme for heterogeneous water percolation in SNOWPACK for both MB and RE [*Wever et al.*, 2015]. Energy inputs at the snow surface promote melt and consequently outflow, which is measured at the lysimeter. As preferential flow is only wetting parts of the snowpack, lower θ_w values and slow increases in θ_w are expected, which is shown in the radar data.

4.4. Comparison of Simulated and Measured Outflow at the Flat Site WFJ

Table 1 compares model results to measured outflow from a lysimeter. All model predictions are presented for a normalized surface area of 1 m^2 per 24 h. The cumulative sums of deviations per season are calculated for simulations subtracted by measured values. Positive values denote that the respective model is overestimating actual values.

Considering cumulative deviations, the knowledge of residual liquid water resisting gravitational flow overall improves model results (Table 1). This is in line with the study by *Essery et al.* [2013]. In all cases, M_S deviations are reduced by subtracting $\hat{m}_{wi}$. The temperature index method (M_D) is improved in five cases. Average offsets in percent for all four spring seasons (only for the reliable "corr" data sets; Table 1) proof that the corrections for residual water masses (M_{SR} and M_{DR}) result in the most accurate outflow estimations. M_{SR} reduces offsets to measured outflow from 18.0% to 6.2% and M_{DR} from 6.29% to 6.25%. Differences between M_{DR}, M_D, and M_{SR} are very small. Occasionally, the performance of the temperature index model corrected for residual water is only slightly improved by correction for radar-determined $\hat{m}_{wi}$. This finding is related to the observation period in 2013 at the WFJ, when the correction of M_D with radar-determined $\hat{m}_{wi}$ decreased predicted outflow sums from −3.3 kg m^{-2} to −59.3 kg m^{-2}. Cumulative offsets for SNOWPACK simulations are comparably large (M_{MB} = 14.3%, M_{RE} = 20.2%). The multilayer bucket simulations hardly differ from results for the single-layer approach (M_{SB} = 12.1%; Table 1). Implementing RE in SNOWPACK results in the largest seasonal offsets of all models for each season—except for spring 2011. For this specific melt season, M_{RE} deviates only slightly from lysimeter data.

Absolute differences in root-mean-square (RMS) values reflect average diurnal deviations of the respective model (Table 2). Again, full energy balance used as input to calculate melt results in significantly lower RMS deviations in kg m^{-2}. The one-dimensional snow cover model SNOWPACK shows the lowest average deviations per day. Especially implementing RE into SNOWPACK increases the model performance. Stratigraphy differences within the snow cover level out as the melt season advances. As a consequence, absolute deviations to measured outflow between single-layer or multilayer bucket approaches are hardly recognizable (Table 2). Considering all four melt seasons, implementing determined changes in residual liquid water does not improve average model performance in terms of RMS deviation. Especially for the melt seasons 2011 and 2013, when lysimeter data are influenced by lateral flow, the incorporation of radar-determined θ_w in, both, temperature index-based and energy balance-based methods cause strong outliers, which influence respective RMS values.

The very low cumulative deviations in total outflow per season for the temperature index method are related to the calibration time. At the flat site WFJ, the degree-day factor has been calibrated over 28 years. Such long data records are very rare and consequently the accuracy of the temperature index model depends strongly on an optimized factor. For most remote sites, neither lysimeter data nor longtime observations exist to optimize the factor. One contributing factor for the largest cumulative offsets of the most physically based and most sophisticated modeling approach is that SNOWPACK continuously underestimates maximum θ_w values for all four seasons. If the holding capacity of the bulk snowpack is underestimated, outflow will be overestimated. This is documented through the consistently largest positive deviations for M_{RE} in Table 1 and the significant underestimation of seasonal maximum θ_w values in Figure 8c. Regarding cumulative sums, such a continuous outflow overestimation will produce large offsets, despite the fact that absolute errors on a daily basis are lowest for the RE approach in SNOWPACK. The observations during the melt period in 2011 contradict

this statement. However, the occurrences of lateral flow and probably not proper correction of it through the presented lysimeter data quality check certainly influence results for the whole observation period.

Simple energy budget and temperature index models are not capable to predict correct first arrivals of liquid water at the snow-ground interface. Simulations based on M_S just consider heat conduction initialized at the surface. The temperature distribution in the whole snowpack before melt is not accounted for, neither the release of latent heat during refreezing. The one-dimensional model SNOWPACK including the RE implementation is most accurate in predicting the start of outflow from the snow cover. However, we observe a delay of at least 1 to 2 days (spring 2011 is considered to be an exceptional case).

5. Conclusions

This study investigates temporal changes of θ_w in natural snowpacks at a flat site and for slopes over multiple melt seasons. Statistical values on temporal evolutions for θ_w during a day and for entire melt periods differ between slopes and the flat site. Diurnal increases in θ_w do not exceed 1.7 vol % at the flat site. On slopes, we observe larger diurnal enhancements. Regarding seasonal cycles, in 90% of data, θ_w values do not exceed 4–5 vol % at the flat site. For the slope sites, 90% of θ_w data are usually below 3.5 vol %.

We compare these records with outputs of two different water transport schemes of the one-dimensional snow cover model SNOWPACK. The implementation of Richards equation in SNOWPACK leads to a very high agreement with radar observations for diurnal variations. A multilayer bucket approach, in contrast, results in much lower diurnal dynamics and consequently underestimates maximum diurnal changes in θ_w, mainly for the flat site. Both model approaches in SNOWPACK underestimate maximum θ_w in the course of a season for the flat site and thus only provide a limited representation of seasonal trends. Most likely, this underestimation is systematic due to undervaluing the effect of water storage at capillary barriers. On slopes lateral flow decreases the influence of such boundary effects.

We demonstrated that on average, for temperature index and energy balance models, cumulative runoff estimates improve if knowledge of changes in water retention is included. For our data with a temporal resolution of 24 h, a simple single-layer bucket model performs equally accurate as the more sophisticated SNOWPACK model requiring various input parameters. In addition, a well-tuned temperature index model simulates seasonal outflow very accurately. Using Richards equation in SNOWPACK decreases mean absolute deviations to measurements. However, when integrated over a full season, outflow sums are highly overestimated. This follows from continuously underestimating θ_w at the flat site.

A next step to improve our understanding of liquid water percolation in snow and firn would be to implement the measurement setup in polar regions, for instance, in locations with perennial firn. Since lysimeter installations are impossible in such regions, upGPR might be the best choice to provide data, which help to optimize model performance and clarify required levels of sophistication of models to assess outflow and liquid water contents accurately.

Notation

upGPR	upward looking ground-penetrating radar.
θ_w	bulk volumetric liquid water content in vol %.
θ_{wi}	irreducible bulk volumetric liquid water content in vol %.
θ_{mi}	irreducible bulk gravitational liquid water content in kilograms.
DS	total thickness of snow pack—measured slope perpendicular in meters.
m_w	mass of liquid water in the snow cover per imaged radar volume in kilograms.
WFJ	flat study site Weissfluhjoch, above Davos, Switzerland.
DFB	sloped study site Dorfberg, above Davos, Switzerland.
BB	sloped study site Bogus Basin, above Boise, Idaho, USA.
τ	radar-measured two-way travel time in nanoseconds.
$\varepsilon_s, \varepsilon_i, \varepsilon_a, \varepsilon_w$	relative dielectric permittivity of snow, ice, air, and water.
θ_i, θ_a	volume fractions of ice and air.
β	exponent for the three-phase mixing formulation.
ρ_s	density of snow in kg m^{-3}.
c_1, c_2, c_3, c_4	empirically determined constants.

$\Delta\theta_{w-max}$	maximum increase of θ_w per day.
A_{surf}	radar illuminated surface area in m^2.
V_{cone}	radar illuminated cone volume in m^3.
V_{cyl}	cylinder volume for given A_{surf} and DS in m^3.
f_{vol}	quotient of V_{cyl} divided by V_{cone}.
$\hat{m}_w$	mass of liquid water per volume per 1 m^2 surface area.
$\hat{m}_{wi}$	mass of irreducible water per volume per 1 m^2 surface area within 24 h time period.
AWS	automatic weather station.
T_A	air temperature.
T_{avg}	daily mean of positive air temperatures.
DDF	degree-day factor.
M_D	daily snow melt calculated from a temperature index model with a calibrated degree-day factor in kg m^{-2} d^{-1}.
M_{DR}	simulated diurnal outflow in kg m^{-2} d^{-1} from daily snow melt (M_D) corrected for radar-determined changes in $\hat{m}_{wi}$.
M_S	daily snow melt calculated from determined net energy inputs per day in kg m^{-2} d^{-1}.
M_{SR}	simulated diurnal outflow in kg m^{-2} d^{-1} from daily snow melt (M_S) corrected for radar-determined changes in $\hat{m}_{wi}$.
M_{SB}	simulated diurnal outflow in kg m^{-2} d^{-1} from daily snow melt (M_S) combined with a single-layer bucket approach to account for changes in residual water.
M_{MB}	predicted diurnal outflow in kg m^{-2} d^{-1} from the one-dimensional model SNOWPACK utilizing a multilayer bucket approach for simulating water transport in snow.
M_{RE}	predicted diurnal outflow in kg m^{-2} d^{-1} from the one-dimensional model SNOWPACK utilizing Richards equation for simulating water transport in snow.
$Q_c(z,t)$	heat flux going into the snow cover in W m^{-2}.
k_{eff}	thermal conductivity of snow in W m^{-1} K^{-1}.
L_i	latent heat of fusion of ice in J kg^{-1}.
LO	lysimeter-measured runoff sums per day in kg m^{-2} d^{-1}.
ρ_{lysi}	mean density for melted snow masses at the WFJ per day in kg m^{-3}.
RMS	root-mean-square.
λ	wavelength in meters.

Acknowledgments

The research project was completed within the framework of the D-A-CH consortium (DFG-FWF-SNF) with the Deutsche Forschungsgemeinschaft (DFG) as lead agency, NSF grant "Lateral Flow of Water in Snow," and NASA grant "Remote Sensing of the Cryosphere." A.H. was supported by DFG grant EI 672/6, and L.S. was funded by the Swiss National Science Foundation (SNF) and O.E. by the DFG Emmy Noether programme grant EI 672/5. For field assistance, we thank Samantha Evans, Andrew Hedrick, Scott Havens, Stephan Simioni, Fabiano Monti, Anna Haberkorn, and several other SLF staff members. The data set used for this study is available upon request from the corresponding author.

References

Baggi, S., and J. Schweizer (2009), Characteristics of wet-snow avalanche activity: 20 years of observations from a high alpine valley (Dischma, Switzerland), *Nat. Hazards*, *50*(1), 97–108, doi:10.1007/s11069-008-9322-7.

Bartelt, P., and M. Lehning (2002), A physical SNOWPACK model for the Swiss avalanche warning, *Cold Reg. Sci. Technol.*, *35*(3), 123–145, doi:10.1016/S0165-232X(02)00074-5.

Braithwaite, R. J. (1995), Positive degree-day factors for ablation on the Greenland ice-sheet studied by energy-balance modeling, *J. Glaciol.*, *41*, 153–160.

Calonne, N., F. Flin, S. Morin, B. Lesaffre, S. Rolland du Roscoat, and C. Geindreau (2011), Numerical and experimental investigations of the effective thermal conductivity of snow, *Geophys. Res. Lett.*, *38*, L23501, doi:10.1029/2011GL049234.

Colbeck, S. (1997), A review of sintering in seasonal snow, CRREL Rep. 97-10, US Army Cold Reg. Res. and Eng. Lab., Hanover, N. H.

Coleou, C., and B. Lesaffre (1998), Irreducible water saturation in snow: Experimental results in a cold laboratory, *Ann. Glaciol.*, *26*, 64–68.

Conway, H., and C. Raymond (1993), Snow stability during rain, *J. Glaciol.*, *39*(133), 635–642.

Daniels, D. J. (2004), *Ground Penetrating Radar, IEE Radar, Sonar, Navigation, and Avionics Ser.*, vol. 15, 2nd ed., Inst. of Electr. Eng., London.

Denoth, A. (1994), An electronic device for long-term snow wetness recording, *Ann. Glaciol.*, *1993*(19), 104–106.

De Michele, C., F. Avanzi, A. Ghezzi, and C. Jommi (2013), Investigating the dynamics of bulk snow density in dry and wet conditions using a one-dimensional model, *Cryosphere*, *7*(2), 433–444, doi:10.5194/tc-7-433-2013.

de Quervain, M. (1979), Schneedeckenablation und Gradtage im Versuchsfeld Weissfluhjoch, *Mitt. VAW/ETH Zürich*, *41*, 215–232.

Eiriksson, D., M. Whitson, C. H. Luce, H. P. Marshall, J. Bradford, S. G. Benner, T. Black, H. Hetrick, and J. P. McNamara (2013), An evaluation of the hydrologic relevance of lateral flow in snow at hillslope and catchment scales, *Hydrol. Processes*, *27*(5), 640–654, doi:10.1002/hyp.9666.

Essery, R., S. Morin, Y. Lejeune, and C. Ménard (2013), A comparison of 1701 snow models using observations from an alpine site, *Adv. Water Resour.*, *55*, 131–148, doi:10.1016/j.advwatres.2012.07.013.

Fierz, C., R. Armstrong, Y. Durand, P. Etchevers, E. Greene, D. McClung, K. Nishimura, P. Satyawali, and S. Sokratov (2009), *The International Classification For Seasonal Snow On The Ground, IACS Contribution*, vol. 1, UNESCO/IHP, Paris.

Gascon, G., M. Sharp, D. Burgess, P. Bezeau, A. B. Bush, S. Morin, and M. Lafaysse (2014), How well is firn densification represented by a physically based multilayer model? Model evaluation for Devon Ice Cap, Nunavut, Canada, *J. Glaciol.*, *60*(222), 694–704, doi:10.3189/2014JoG13J209.

Gupta, R. P., U. K. Haritashya, and P. Singh (2005), Mapping dry/wet snow cover in the Indian Himalayas using IRS multispectral imagery, *Remote Sens. Environ.*, *97*(4), 458–469, doi:10.1016/j.rse.2005.05.010.

Harper, J., N. Humphrey, W. T. Pfeffer, J. Brown, and X. Fettweis (2012), Greenland ice-sheet contribution to sea-level rise buffered by meltwater storage in firn, *Nature*, *491*(7423), 240–243, doi:10.1038/nature11566.
Heilig, A., M. Schneebeli, and O. Eisen (2009), Upward-looking ground-penetrating radar for monitoring snowpack stratigraphy, *Cold Reg. Sci. Technol.*, *59*(2–3), 152–162, doi:10.1016/j.coldregions.2009.07.008.
Heilig, A., O. Eisen, and M. Schneebeli (2010), Temporal observations of a seasonal snowpack using upward-looking GPR, *Hydrol. Processes*, *24*(22), 3133–3145, doi:10.1002/hyp.749.
Heilig, A., H. P. Marshall, and S. Evans (2012), Temporal and spatial changes of a seasonal snowpack within a small sheltered slope, paper presented at 2012 International Snow Science Workshop. Anchorage, Alaska, pp. 1069–1074, 16–21 Sept.
Jones, E., A. Rango, and S. Howell (1983), Snowpack liquid water distributions using freezing calorimetry, *Nord. Hydrol.*, *14*, 113–126.
Juen, M., C. Mayer, A. Lambrecht, H. Han, and S. Liu (2014), Impact of varying debris cover thickness on ablation: A case study for Koxkar Glacier in the Tien Shan, *Cryosphere*, *8*(2), 377–386, doi:10.5194/tc-8-377-2014.
Kattelmann, R., and J. Dozier (1999), Observations of snowpack ripening in the Sierra Nevada, California, U.S.A., *J. Glaciol.*, *45*(151), 409–416.
King, J., J. Pomeroy, D. Gray, C. Fierz, P. Fohn, R. Harding, R. Jordan, E. Martin, and C. Plüss (2008), Snow-atmosphere energy and mass balance, in *Snow and Climate: Physical Processes, Surface Energy Exchange and Modeling*, edited by R. L. Armstrong and E. Brun, pp. 70–124, Cambridge Univ. Press, Cambridge, U. K.
Lehning, M., P. Bartelt, B. Brown, C. Fierz, and P. Satyawali (2002a), A physical SNOWPACK model for the Swiss avalanche warning: Part II. Snow microstructure, *Cold Reg. Sci. Technol.*, *35*(3), 147–167, doi:10.1016/S0165-232X(02)00073-3.
Lehning, M., P. Bartelt, B. Brown, and C. Fierz (2002b), A physical SNOWPACK model for the Swiss avalanche warning: Part III: Meteorological forcing, thin layer formation and evaluation, *Cold Reg. Sci. Technol.*, *35*(3), 169–184, doi:10.1016/S0165-232X(02)00072-1.
Lehning, M., P. Bartelt, B. Brown, and C. Fierz (2002c), A physical SNOWPACK model for the Swiss avalanche warning, *Cold Reg. Sci. Technol.*, *35*(3), 169–184, doi:10.1016/S0165-232X(02)00072-1.
Luce, C. H., and D. G. Tarboton (2010), Evaluation of alternative formulae for calculation of surface temperature in snowmelt models using frequency analysis of temperature observations, *Hydrol. Earth Syst. Sci.*, *14*, 535–543.
Marty, C., and R. Meister (2012), Long-term snow and weather observations at Weissfluhjoch and its relation to other high-altitude observatories in the Alps, *Theor. Appl. Climatol.*, *110*(4), 573–583, doi:10.1007/s00704-012-0584-3.
Maurer, G. E., and D. R. Bowling (2014), Seasonal snowpack characteristics influence soil temperature and water content at multiple scales in interior western U.S. mountain ecosystems, *Water Resour. Res.*, *50*, 5216–5234, doi:10.1002/2013WR014452.
Mitterer, C., H. Hirashima, and J. Schweizer (2011a), Wet-snow instabilities: Comparison of measured and modelled liquid water content and snow stratigraphy, *Ann. Glaciol.*, *52*(58), 201–208, doi:10.3189/172756411797252077.
Mitterer, C., A. Heilig, J. Schweizer, and O. Eisen (2011b), Upward-looking ground-penetrating radar for measuring wet-snow properties, *Cold Reg. Sci. Technol.*, *69*(2–3), 129–138.
Munneke, P. K., S. R. M. Ligtenberg, M. R. van den Broeke, J. H. van Angelen, and R. R. Forster (2014), Explaining the presence of perennial liquid water bodies in the firn of the Greenland Ice Sheet, *Geophys. Res. Lett.*, *41*, 476–483, doi:10.1002/2013GL058389.
Nagler, T., and H. Rott (2000), Retrieval of wet snow by means of multitemporal SAR data, *IEEE Trans. Geosci. Remote Sens.*, *38*(2), 754–765.
Pfeffer, W. T., M. F. Meier, and T. H. Illangasekare (1991), Retention of Greenland runoff by refreezing: Implications for projected future sea level change, *J. Geophys. Res.*, *96*(C12), 22,117–22,124, doi:10.1029/91JC02502.
Roth, K., R. Schulin, H. Flühler, and W. Attinger (1990), Calibration of time domain reflectometry for water content measurement using a composite dielectric approach, *Water Resour. Res.*, *26*, 226–273.
Schmid, L., C. Mitterer, A. Heilig, J. Schweizer, and O. Eisen (2012), Tracking wetting front advance with upward-looking ground-penetrating radar, paper presented at 2012 International Snow Science Workshop, Anchorage, Alaska, pp. 599–601, 16–21 Sept.
Schmid, L., A. Heilig, C. Mitterer, J. Schweizer, H. Maurer, R. Okorn, and O. Eisen (2014), Continuous snowpack monitoring using upward-looking ground-penetrating radar technology, *J. Glaciol.*, *60*(221), 509–525, doi:10.3189/2014JoG13J084.
Schmid, L., F. Koch, A. Heilig, M. Prasch, O. Eisen, W. Mauser, and J. Schweizer (2015), A novel sensor combination (upGPR-GPS) to continuously and non-destructively derive snow cover properties, *Geophys. Res. Lett.*, *42*, 3397–3405, doi:10.1002/2015GL063732.
Schneider, T., and P. Jansson (2004), Internal accumulation in firn and its significance for the mass balance of Storglaciären, Sweden, *J. Glaciol.*, *50*(168), 25–34.
Shi, J., and J. Dozier (1995), Inferring snow wetness using c-band data from the SIR-c's polarimetric synthetic aperture radar, *IEEE Trans. Geosci. Remote Sens.*, *33*(4), 905–914.
Steffen, K., S. V. Nghiem, R. Huff, and G. Neumann (2004), The melt anomaly of 2002 on the Greenland Ice Sheet from active and passive microwave satellite observations, *Geophys. Res. Lett.*, *31*, L20402, doi:10.1029/2004GL020444.
Stössel, F., M. Guala, C. Fierz, C. Manes, and M. Lehning (2010), Micrometeorological and morphological observations of surface hoar dynamics on a mountain snow cover, *Water Resour. Res.*, *46*, W04511, doi:10.1029/2009WR008198.
Techel, F., and C. Pielmeier (2011), Point observations of liquid water content in wet snow—Investigating methodical, spatial and temporal aspects, *Cryosphere*, *5*(2), 405–418, doi:10.5194/tc-5-405-2011.
Tedesco, M., X. Fettweis, T. Mote, J. Wahr, P. Alexander, J. E. Box, and B. Wouters (2013), Evidence and analysis of 2012 Greenland records from spaceborne observations, a regional climate model and reanalysis data, *Cryosphere*, *7*(2), 615–630, doi:10.5194/tc-7-615-2013.
van Pelt, W. J. J., R. Pettersson, V. A. Pohjola, S. Marchenko, B. Claremar, and J. Oerlemans (2014), Inverse estimation of snow accumulation along a radar transect on Nordenskiöldbreen, Svalbard, *J. Geophys. Res. Earth Surf.*, *119*, 816–835, doi:10.1002/2013JF003040.
Waldner, P. A., M. Schneebeli, U. Schultze-Zimmermann, and H. Flühler (2004), Effect of snow structure on water flow and solute transport, *Hydrol. Processes*, *18*(7), 1271–1290, doi:10.1002/hyp.1401.
Wever, N., C. Fierz, C. Mitterer, H. Hirashima, and M. Lehning (2014), Solving Richards equation for snow improves snowpack meltwater runoff estimations in detailed multi-layer snowpack model, *Cryosphere*, *8*(1), 257–274, doi:10.5194/tc-8-257-2014.
Wever, N., L. Schmid, A. Heilig, O. Eisen, C. Fierz, and M. Lehning (2015), Verification of the multi-layer SNOWPACK model with different water transport schemes, *Cryosphere Discuss.*, *9*, 2655–2707, doi:10.5194/tcd-9-2655-2015.
Wilhelms, F. (2005), Explaining the dielectric properties of firn as a density-and-conductivity mixed permittivity (decomp), *Geophys. Res. Lett.*, *32*, L16501, doi:10.1029/2005GL022808.
Yamaguchi, S., K. Watanabe, T. Katsushima, A. Sato, and T. Kumakura (2012), Dependence of the water retention curve of snow on snow characteristics, *Ann. Glaciol.*, *53*(61), 6–12, doi:10.3189/2012AoG61A001.